THE ASTROPHYSICAL JOURNAL, 467:881–886, 1996 August 20

DIFFERENTIAL MAGNETIC FIELD SHEAR IN AN ACTIVE REGION

B. SCHMIEDER,[1] P. DÉMOULIN,[1] G. AULANIER,[1] AND L. GOLUB[2]
Received 1995 December 1; accepted 1996 March 7

ABSTRACT

The three-dimensional extrapolation of magnetic field lines from a magnetogram obtained at Kitt Peak allows us to understand the global structure of the NOAA active region 6718, as observed in X-rays with the Normal Incidence X-ray Telescope (NIXT) and in Hα with the Multichannel Subtractive Double Pass spectrograph (MSDP) in Meudon on 1991 July 11. This active region was in a quiet stage. Bright X-ray loops connect plages having field strengths of ~300 G, while Hα fibriles connect penumbrae having strong spot fields to the surrounding network. Small, intense X-ray features in the moat region around a large spot, which could be called X-ray–bright points, are due mainly to the emergence of magnetic flux and merging of these fields with surrounding ones. A set of large-scale, sheared X-ray loops is observed in the central part of the active region. Based on the fit between the observed coronal structure and the field configurations (and assuming a linear force-free field), we propose a *differential magnetic field shear* model for this active region. The decreasing shear in outer portions of the active region may indicate a continual relaxation of the magnetic field to a lower energy state in the progressively older portions of the AR.

Subject headings: MHD — Sun: faculae, plages — Sun: magnetic fields

1. INTRODUCTION

Because of the high conductivity of the coronal plasma along magnetic field lines, and because of the low β of the plasma, the structure in an active region is determined largely by the magnetic field. Observations of the magnetic field in the photosphere is commonly based on the splitting of lines due to the Zeeman effect. At the photospheric level, only the distribution of magnetic flux is measured, while the field topology (field line connectivity) is difficult to establish from the photospheric field measurements. Although some high-resolution microwave interferometry is beginning to be used to deduce the magnetic structure in the corona, it is still necessary to assume a model for both the coronal field and plasma. Alternatively, to infer the large-scale three-dimensional structure at heights above those at which the magnetograph measurements are made (>1000 km) we can extrapolate the measured photospheric field (Alissandrakis 1981; Sakurai 1982; Hannakam, Gary, & Teuber 1984) using a variety of successively more elaborate methods. If any currents in the region are confined to heights at or below the photosphere, the field above is a potential field. If not, a force-free field configuration ($\boldsymbol{J} \times \boldsymbol{B} = \boldsymbol{0}$, $\nabla \times \boldsymbol{B} = \alpha \boldsymbol{B}$) is commonly assumed because of the low plasma β, corresponding to $\boldsymbol{J} \parallel \boldsymbol{B}$.

This theoretical assumption has recently received support from observations: Metcalf et al. (1995) show, by computation of the magnetic field from the Stokes parameters observed in the Na I line, that the photospheric field is not force free but that it becomes force free roughly 400 km above the photosphere in a quiet active region.

There have been only a limited number of attempts in recent years to carry out direct comparisons between high-resolution coronal observations and magnetic field extrapolations. Several attempts have been made to explain the onset of flares by testing the nonpotentiality of the fields. Typically, $B_\perp$ is compared with Hα fibrils (Schmieder et al. 1990) or Lyα fibrils (Gary et al. 1987). For nonflaring regions, only a few attempts have been made. Poletto et al. (1975), and Sakurai & Uchida (1977) successfully modeled some connected active regions observed with *Skylab* by using potential extrapolations of photospheric fields, and Sams, Golub, & Weiss (1992) confirmed a general agreement by using NIXT observations. Recently, McClymont & Mikic (1994) used a three-dimensional magnetohydrodynamic (MHD) code to analyze a highly sheared region; they found that, in agreement with observations, the highly sheared loops should have a thickness variation along their lengths of only 10%–20%.

It is reasonable to ask whether we always need such a huge code and supercomputer resources to analyze the magnetic fields of active regions. Do less sophisticated methods of extrapolation, which are much faster and more economical, give some insight into the observations? In the present study, we use a linear force-free field extrapolation, discuss its limitations, and show that some significant insights can be gained in understanding the observation. In particular, we may ask how the observed coronal loops correspond to the extrapolated magnetic field lines under this hypothesis and why the connectivity of the X-ray–bright structures follows the topology which is observed.

For this study, we have available a set of high-resolution data sets of a "quiet" active region in Hα obtained with the Meudon MSDP, in soft X-ray observed by NIXT, and magnetic data from Kitt Peak. We have compared extrapolated magnetic field lines above the AR 6718 on 1991 July 11 with cold and hot structures by using Hα fibrils and filaments (MSDP) and X-ray loops (NIXT).

2. INSTRUMENTS

2.1. *NIXT*

The Normal Incidence X-ray Telescope (NIXT) was launched on a NASA sounding rocket 1991 July 11 at 17:25 UT, during a solar eclipse. The NIXT instrument observes

[1] Observatoire de Paris, Section de Meudon, URA 2080, 92195 Meudon, Cedex Principal, France.
[2] Smithsonian Astrophysical Observatory, Harvard-Smithsonian Center for Astrophysics, Cambridge, MA 02138.

the full disk with a resolution less than 1″; it is described in detail by Spiller et al. (1991). The multilayer mirror has a passband of 1.4 Å at 63.5 Å corresponding to two coronal lines, one of Mg X and one of Fe XVI, formed at $T \sim 1 \times 10^6$ K and 3×10^6 K, respectively. The brightening of Mg X occurs near loop footpoints and often coincides with bright chromospheric regions of higher magnetic field strength (network, plages) and of higher density (Peres, Reale, & Golub 1994; Golub, Zirin, & Wang 1994). The brightening is caused by the presence at the loop footpoint of $T \sim 10^6$ K material with sufficient emission measure to produce a visible brightening. This is found to occur typically in the higher pressure coronal loops. Four long-exposure (30 and 60 s) images were obtained between 17:27:11 UT and 17:30:45 UT. For the present study, we use the same notation to identify the main X-ray structures (B, C, E, W) as Golub et al. did.

2.2. *MSDP*

On July 11 the Multichannel Subtractive Double Pass (MSDP) spectrograph was operating at the Meudon Solar Tower. Its good spatial resolution (1″–1″.5) allows us to see the fine chromospheric structures: fibrils and filaments which will be used for coalignment with the extrapolated magnetic field lines. The MSDP provides nine different wavelength channels of the same two-dimensional area of the Sun (Mein 1977). Some details of the data reduction procedures have been presented in Schmieder, Golub, & Antiochos (1994). The data allow us to reconstruct by interpolation a line profile for each pixel in the field of view. For a given chord ($\Delta\lambda$), the intensity is computed in each pixel, and maps of intensities can be displayed. The standard value for $\Delta\lambda$ is taken equal at 0.6 Å, which corresponds commonly to the half-width of the Hα profile at which the contrast of chromospheric fine structures is generally the best.

2.3. *Magnetograph*

The magnetograph of the Kitt Peak National Observatory has been described by Livingston et al. (1976). It provides daily full-disk longitudinal magnetic field maps. We use a magnetogram taken on July 11 at 15:55 UT in the 868.8 nm line (Fig. 1*b* [Pl. 6]). This observation is used for computing the coronal magnetic field lines by extrapolation (see next section). The spatial resolution of the magnetogram is around 1″. The saturation level of the instrument is about 9000 G; however, because of scattered light, the response of the system inside sunspot umbras was reduced by about a factor of 1.5 (J. Harvey, private communication). Taking this correction into consideration in the spots does not change significantly the extrapolated field lines related to the X-ray–bright loops.

3. ACTIVE REGION 6718

AR 6718 during its disk passage was followed by Debrecen and Potsdam observatories (Aurass et al. 1993). AR 6718 appeared at the east limb as a fairly regular bipolar group, consisting of a round middle-sized spot on the preceding end, together with an elongated (NW-SE) following part with several umbrae in a common penumbra on the other end, and some pores in the middle of the group. The most stable two umbrae are named P0 and F0, as shown in Figure 1*a*. On July 7, F0 is separated from the rest of the chain by a light bridge, while the other umbrae of the following part gradually decrease and disperse.

A development of new activity begins from July 8 to 9. In the middle part of the active region, there are new pores forming continually, mostly of positive polarity, which stream forward systematically and eventually coalesce with P0. On July 10, four small umbrae appear and form P1. The counterpart of P1 may be F1 to the south of F0. South of F0, small satellite sunspots of positive polarity emerge, which will correspond to some bright points seen in X-rays during the rocket flight. To the east of F0 we observe a sunspot, P4, which is also associated with X-ray brightenings. At the center of the active region, the small dipole consisting of the pores P2 and F2 is observable only on July 11.

The axis of the new emerging flux regions P1–F1 and P2–F2 has a significant shear compared with the P0–F0 axis (Fig. 2). Their evolution is responsible for the flare occurring on July 10. The greatest evolution is from July 10 to 11 (Aurass et al. 1993). The two ribbons were over P1 and F1, and the flare is likely due to the interaction of P1–F1 with P0–F0. Microwaves at high frequency were recorded. This active region is not very productive of the high level class of flares. Geophysical Data registered the following:

1. July 9, 15:04 M1.2 and some C flares;
2. July 10, 12:26 UT M3.6 and some C flares;
3. July 11, 13:39 and 14:54 UT Hα subflares;
4. July 12, some C flares.

During the NIXT flight, no flares occurred in this region, but sheared bright loops were observed over the active

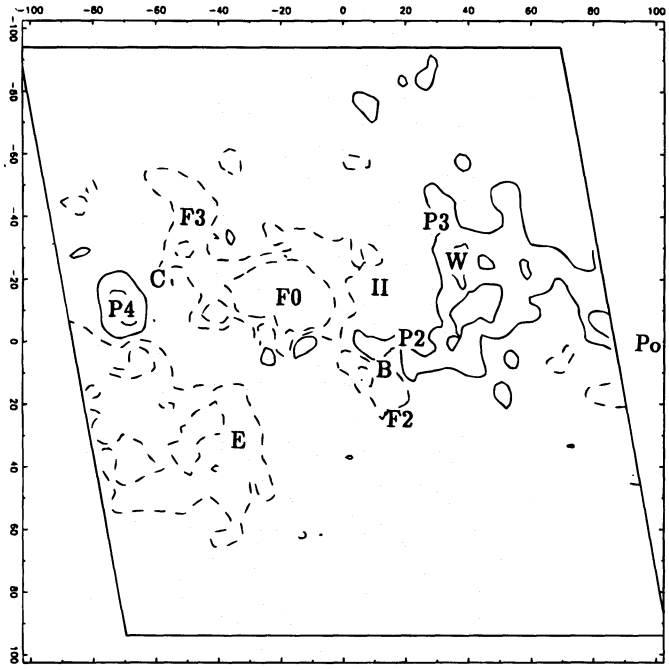

FIG. 2.—Kitt Peak magnetogram of AR 6718 centered on the larger X-ray loops. The labels (P0–P4, F1–F3) designate the sunspots (see Fig. 1) according to their magnetic polarities, "II" locates the Hα filament (from Aurass et al. 1993), while B, C, E, W locate the main X-ray structures (from Golub et al. 1994). Continuous and dashed isoncontours represent the longitudinal photospheric field (100 G, 400 G). The scale length unit is in Megameters. North is to the top. The diamond frame delimits the part of the magnetogram shown in the following figures; its borders are parallel to the local parallel and meridian. The extrapolation computation however, is done for a larger region (400 Mm).

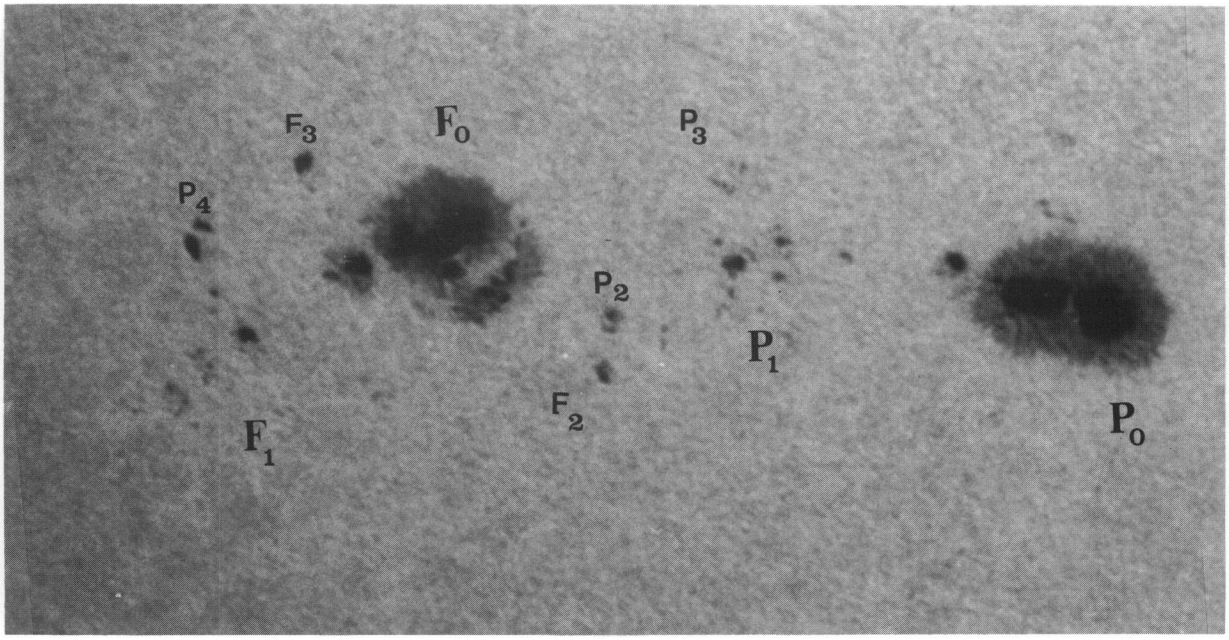

FIG. 1*a*

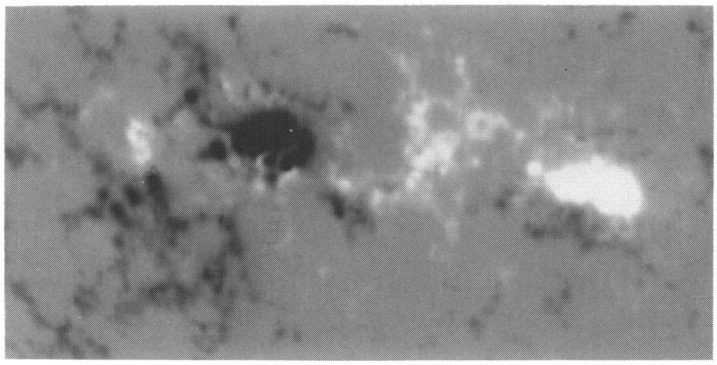

FIG. 1*b*

FIG. 1.—(*a*) White-light image of AR 6718 obtained in Débrecen (courtesy of B. Kalman). The letters indicate the sunspots according to their magnetic polarities and relationship. (*b*) Kitt Peak magnetogram of AR 6718. White/black regions correspond to positive/negative polarities (courtesy of J. Harvey).

region. We propose computing the extrapolated magnetic field in the corona from photospheric observations in order to quantify the shear of the coronal loops observed in X-rays.

4. EXTRAPOLATION OF THE MAGNETIC FIELD

The extrapolation code is based on the work of Alissandrakis (1981). The extrapolated fields are calculated under the linear (or constant α) force-free field assumption ($\nabla \times \boldsymbol{B} = \alpha \boldsymbol{B}$) using a fast Fourier transform method. (Fig. 3). The required boundary condition is a match to the longitudinal magnetic field values at the photosphere. In order to be able to extrapolate the large-scale structures that are the X-ray–bright loops present in AR 6718, a magnetogram with a large field of view is required. We select a region approximately 400 by 400 Mm in the full-disk Kitt Peak magnetogram. In the figures, we show only a fraction of this field of view, corresponding to the large-scale X-ray loops approximately 100 Mm long, but the magnetic computations are always done using the full selected magnetogram region. This extended region was required to take into account the surrounding field and to decrease the aliasing errors at the borders of the computed region (see Alissandrakis 1981).

The use of magnetograms taken away from the solar disk center requires the elimination of projection effects on the magnetic field and on the spatial coordinates. The full transformation method has been discussed by Gary & Hagyard (1990). On this base, Démoulin et al. (1996) have developed a three-dimensional code for magnetic extrapolation; it has been applied to relate Hα flare brightenings to the magnetic topology of the extrapolated field. A more detail discussion of the extrapolation procedure and tests can be found there.

In the present case, the spiral pattern of Hα fibrils indicates that the fields at the chromospheric level are not potential (see Aurass et al. 1993 or Fig. 4*a* [Pl. 7]). The presence of magnetic shear at the coronal level is also evident from the X-ray data (Golub et al. 1994 or Fig. 4*c*). This contrasts with several previous studies, which concluded that quiet coronal structures are well represented by a potential field extrapolation (Poletto et al. 1975; Sams et al. 1992). Therefore, we have investigated the quality of an extrapolation of the magnetogram with increasing values of the shear (Fig. 3). As is evident, the field lines computed from a potential-field approximation cannot represent both the observed Hα and X-ray structures (Figs. 4*a* and Fig. 4*c* respectively). As we impose an increasing positive α, the computed field lines become closer to the observed structures. The combination of Hα (showing mainly low-lying loops or the feet of loops), X-rays (showing the coronal part of the loops, but with a varying sensitivity along the loop), and extrapolation (giving the entire field line but with uncertainties in the modeling) permit a clarification of the magnetic configuration of AR 6718.

Connections between the strongest polarities (P0–F0) are found in the extrapolation. But while this is the most important magnetic linkage in AR 6718 (both in magnetic flux and intensity), there is no detectable enhanced heating associated with it, either at the chromospheric or coronal level. Small emerging flux regions, like P2–F2 which emerged from July 9 to 11 (see Fig. 2), produce higher levels of X-ray emission (see Fig. 4*c*), showing that strong magnetic intensity is not a prime requisite for heating. The magnetic loops connecting P2–F2 were found easily in the extrapolation but not the ones connecting P3 to F3 (suggested by Aurass et al. 1993): field lines starting from P3 always end to the north of F0.

In the east part of the region, both the X-ray (called C in Golub et al. 1994) and Hα brightenings located to the southeast of F3 are related to magnetic field lines linking F3 to the southeast negative polarity (called P4 in Fig. 2). It is probably the emergence of this bipole P3–F3, like in the above case P2–F2, that leads to forced reconnection with the overlying magnetic field. Other smaller examples of this phenomenon, at lower spatial scale length, are present to the south of F0 (see the small positive polarities in Fig. 2, which are located in close proximity to the small X-ray brightenings).

AR 6718 is thus formed by a great number of dipoles of different scales which reconnect and brighten when they find their way into the corona. This explanation can hardly be generalized to the spectacular X-ray loops extending from east to west because the polarities look well formed and the X-ray loops seem to fill a large coronal volume. Hereafter we focus on that large feature, keeping in mind that the intense X-ray feature called B (Fig. 2) is linked to the emergence of polarities P2–F2 and only seems to be cospatial with the loops extending from west to east because of projection effects.

The hot loops extending from west to east can be found in the field line extrapolation when a positive α is introduced (Fig. 3). However, a unique value of α will not fit all the observed structures. Larger and higher structures are found to be less sheared than the lower ones, and even the very low highly sheared structures seen in Hα in the vicinity and in the Hα filament (indicated by II in Fig. 2 and visible in Fig. 4*a*) cannot be reproduced by the extrapolation. Here we see a paradox between the observations and the linear force-free field model. An intrinsic property of the linear force-free field is that large structures are more sheared than smaller ones, implying that long field lines become unrealistically distorted as α is increased (Fig. 3), while short low-lying loops cannot be made as sheared as they are observed to be. The comparison of observations to the extrapolation shows that the coronal magnetic field is not in a state of minimum energy (which is a linear force-free field keeping the total magnetic helicity preserved).

Within the limits of the constant α hypothesis, we can nevertheless reproduce the observed shape of the X-ray loops. The lower loops, corresponding to the dash-dotted curves in Figure 4*b*, are reproduced in the extrapolation by using $\alpha = 0.019$ Mm^{-1}. The larger loops, corresponding to the continuous curves in Figure 4*b*, are approximately reproduced in the extrapolation with $\alpha = 0.013$ Mm^{-1} ($\approx$30% less than the value requires for the lower X-ray loops). These loops are still highly sheared, and they extend to a large altitude (between 60 and 100 Mm). One can imagine that there are magnetic loops which extend even higher, becoming progressively closer to the potential case, but that such loops are not bright enough to be seen in X-rays. A simplified model of this region is a system of magnetic arcades, highly sheared in the center and becoming progressively less sheared outward (Fig. 5). This is in agreement with the schematic view of the magnetic configuration that Martin (1990) proposed for magnetic configurations supporting filaments.

But why are the loops that extend from west to east bright in X-rays? The brightness of the footpoints both in

PLATE 7

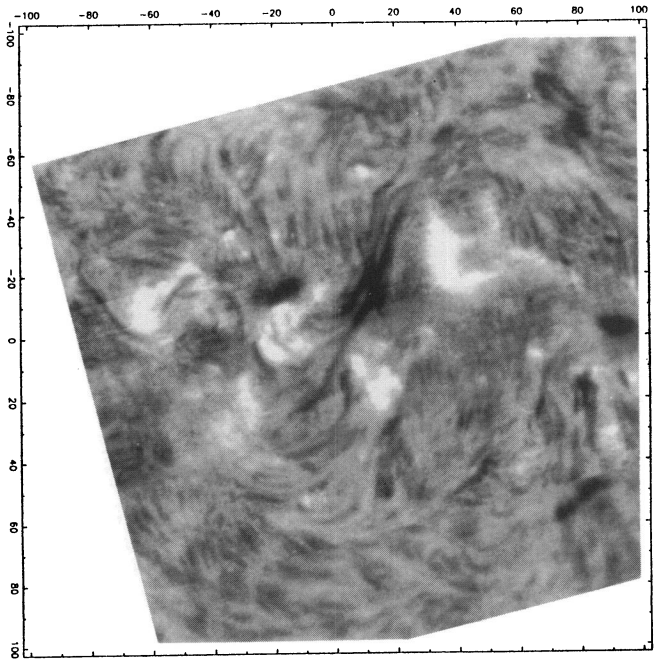

FIG. 4*a*

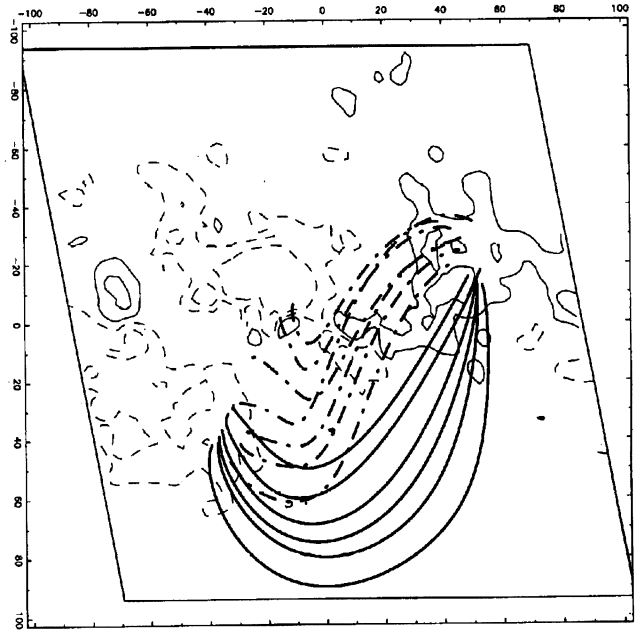

FIG. 4*b*

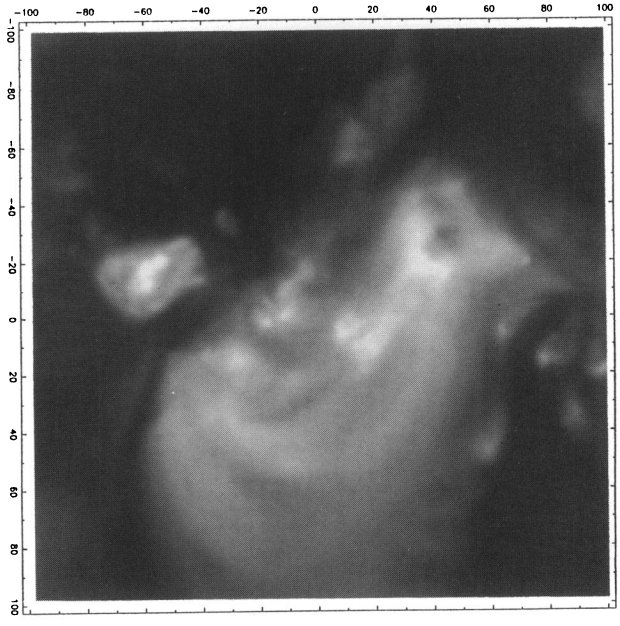

FIG. 4*c*

FIG. 4.—Comparison of (*a*) the MDSP and (*c*) the NIXT observations of AR 6718 to (*b*) the field line computation. The computed field lines (drawn in continuous style) have a shape compatible with the largest X-ray–bright loops only when a sheared field is used ($\alpha = 0.013$ Mm^{-1}). The interpretation of the shape of the lower X-ray loops by field lines (drawn in dash-dotted style) requires a slightly more sheared field ($\alpha = 0.019$ Mm^{-1}). The degree of magnetic shear decreases with height from the lower highly sheared Hα loops (*a*) to the higher coronal loops (*c*).

SCHMIEDER et al. (see 467, 883)

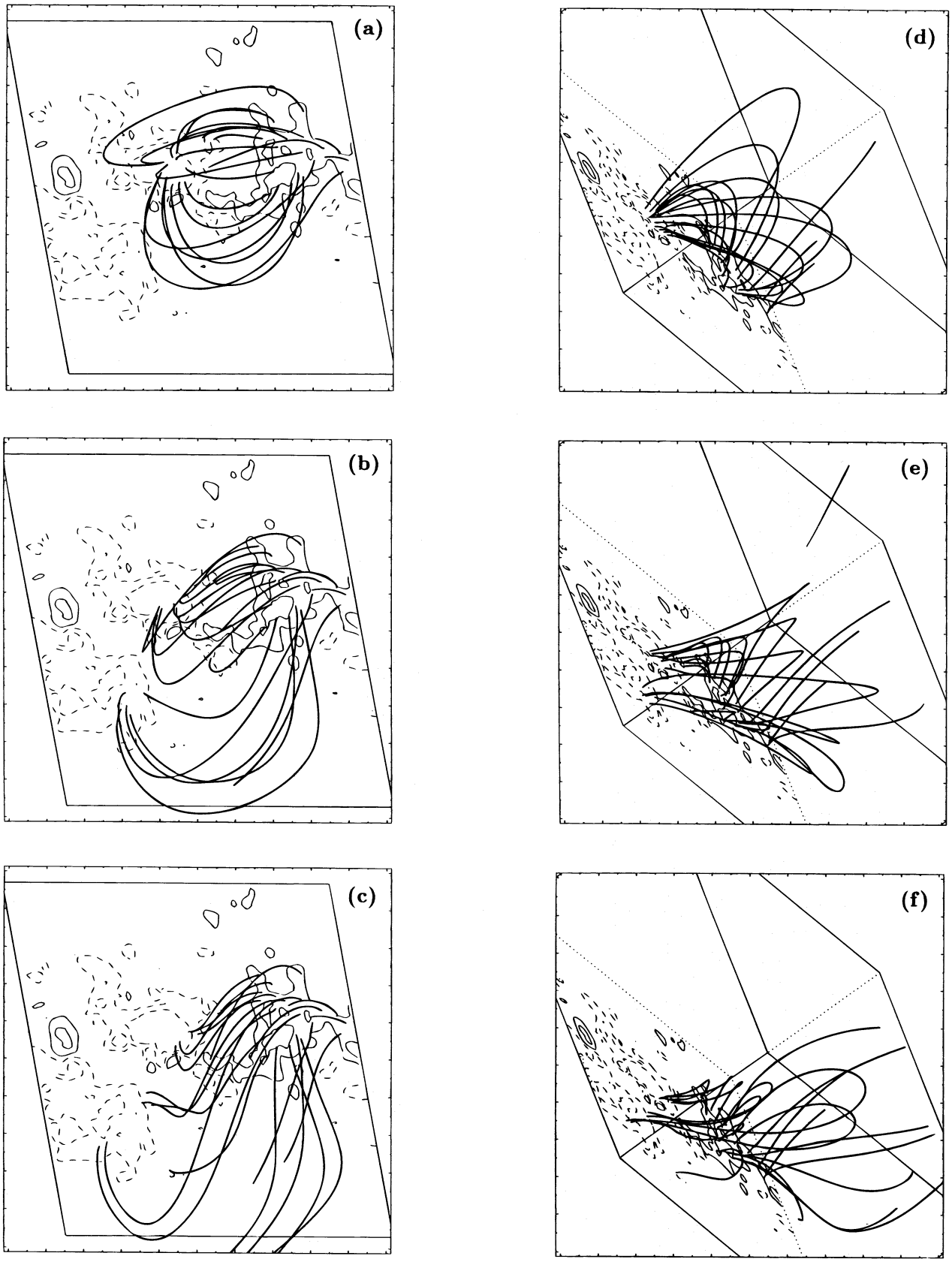

FIG. 3.—Extrapolation of a Kitt Peak magnetogram of the AR 6718 with (*a*, *d*) a potential field and a linear force-free field with (*b*, *e*) $\alpha = 0.013$ Mm^{-1} and (*c*, *f*) $\alpha = 0.019$ Mm^{-1}. Field lines have the same starting footpoint in the positive polarity. In (*a*–*c*), the point of view of the observer is used (north is to the top), while in (*d*–*f*) a side view is shown with the same field lines. The drawing convention for the longitudinal field is the same as in Fig. 2. Only a local view of the region is shown, but the extrapolation is made on a region 4 times larger.

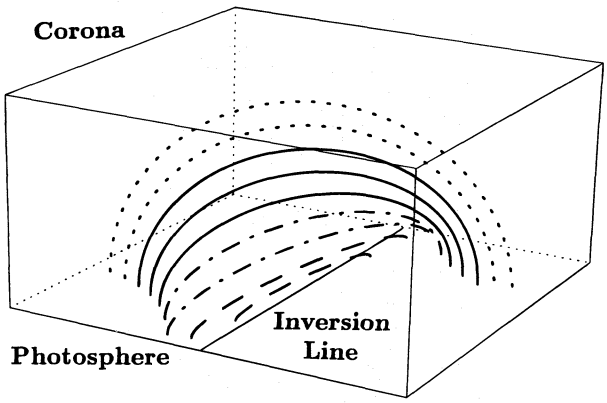

FIG. 5.—Schematic view of the magnetic configuration of AR 6718. The prominence is present in low-lying highly sheared loops (*dashed lines*), surrounded by arcade loops with magnetic shear decreasing with height (field lines corresponding to the observed X-ray coronal loops are drawn with dash-dotted and continuous lines, while the supposed overlying more potential field lines are drawn with dotted lines).

Hα and X-rays delineates approximately the magnetic field map, in particular for the characteristic shape of P3 (Fig. 4). But we have seen above (for loops connecting P0 to F0) that the magnetic field strength is not sufficient to determine the X-ray brightness. The shape of the loop footpoints tells us only that the energy is of magnetic origin and that some other physical parameters should play a key role. It could be the topology of the magnetic field: it is well known that magnetic reconnection occurs on separatrices (see, e.g., Van den Oord 1993; Démoulin 1994). Therefore, we have tried an analysis similar to the one carried out for flares (Démoulin et al. 1996), but without success. This may indicate that the magnetic topology is not well represented by our computation in this highly sheared region (in particular because magnetic shear decreases with height, while the opposite occurs in the linear force-free field extrapolation). But, rather than a localized emission on some loops (or flat volume), the observed X-ray loops on July 11 are seen in a large volume. Another possibility, as suggested in a recent study by Moore et al. (1994), is that X-ray loops are heated at the places at which high shear is present and where underlying flux cancellation occurs. In the present event, flux cancellation may happen in the small bipole (P2–F2) under the large-scale X-ray loops, but it is difficult to believe that such localized and low-lying phenomena can trigger magnetic energy release in the whole large-scale set of X-ray loops.

Rather, we propose that the origin of the observed brightenings of the strongly sheared region are due to the relaxation of the magnetic field as modeled by Heyvaerts & Priest (1984). They described how a magnetic field can lose its excess energy via an MHD turbulent process. In a highly conducting plasma, small-scale processes dissipate magnetic energy much more rapidly than the total magnetic helicity ($H = \int \boldsymbol{A}\boldsymbol{B}\,dV$ with $\boldsymbol{B} = \nabla \times \boldsymbol{A}$; Taylor 1974) or more precisely in the solar context, the total relative helicity (Berger 1985, and references therein). With this constraint, the magnetic field does not relax to a potential state but to a linear force-free state (as was observed in laboratory experiments in spheromacs (Rosenbluth & Bussac 1979). The theoretical final state of the process is a magnetic field with constant α. The gradient of α found in this region (scale length of 100 Mm) shows that the process of relaxation was not complete at the time of the observations.

5. DISCUSSION AND CONCLUSION

We have used a linear-force-free field extrapolation of the longitudinal field to understand the three-dimensional shape of the observed X-ray and Hα structures. The X-ray loops in AR 6718 can be separated in two sets: compact and small loops (with an extension lower than 30 Mm) and large loops (extending to greater than 100 Mm). The emergence of small parasitic polarities and the reconnection of this new magnetic flux with the preexisting coronal magnetic field is the most plausible interpretation for the small-scale X-rays and Hα brightenings. The large-scale X-ray loops are anchored in the bipolar field (P1–F1) located in the middle of a stronger bipolar field (P0–F0). Only a set of loops joining P1 to F1 is observed to be bright in X-rays. These loops cannot be related to field lines in the potential approximation, but we show, in a first approximation, that a constant α force-free field extrapolation permits their shape to be recovered, and it shows that the large-scale X-ray loops are highly sheared. However, a second approximation step shows that a different α value is required to fit the field lines both to the lower and upper parts of the X-ray loops. The upper ones are less sheared; they require an α value approximately 30% smaller than for the lower loops. Moreover, an Hα filament is present below and the Hα fibrils are nearly aligned along the photospheric inversion line, showing that the central part is strongly sheared. Then X-ray and Hα observations combined with the magnetic extrapolation show that the central part of AR 6718 is formed by a highly sheared magnetic field, with a magnetic shear decreasing progressively with height (on a scale height of the order of 100 Mm). Therefore, we propose a differential shear configuration for the magnetic field, with a strongly sheared core (Fig. 5), in agreement with the views of Martin (1990) and Antiochos, Dahlburg, & Klimchuk (1994).

The small-scale X-ray loops can find their origin in the reconnection of parasitic flux with the preexisting magnetic flux, while the brightness of the large-scale X-ray loops is puzzling. In the large-scale magnetic configuration, why are only some loops bright? The magnitude of the magnetic field is not the only important parameter of the heating mechanism, since some parts of the corona have much higher fields while they do not emit in X-rays, and the X-ray–bright loops do not have footpoints in the main sunspots (see also Sams et al. 1992). However, we can surmise that the mechanism is of magnetic origin, since the brighter loops are associated with the photospheric magnetic polarities. Are the observed loops bright due to reconnection between the main bipoles (P0–F0) and (P1–F1)? Within the limits of the magnetogram calibration and the linear force-free field assumption, the topological computations have failed to explain the position of the large X-ray loops. Moreover, the observed spatial extension of the bright loops rules out a mechanism localized on a very flat volume, like reconnection on two intersecting separatrices. The mechanism for heating these quiet X-ray loops seems to be different from that found for flares (Démoulin et al. 1996).

We find that the brightest soft X-ray emission corresponds to a nonpotential state of the magnetic field, in which the strongest X-ray emission is associated with the largest shear (this, however, does not hold for the highly

sheared field lines containing the filament). This agrees with Moore et al. (1994), who report that the coronal heating is enhanced at the sites of strong shear. This argument receives additional indirect support from the measurement of the cross-sectional variation of the loops observed by NIXT (Golub 1991) and by the *Yohkoh* SXT: the thickness variation along the loop was found to be only 10%–20% at most. McClymont & Mikic (1994) demonstrate that this observation is consistent with the characteristics of current carrying field lines in a highly sheared active region (using an MHD code for the extrapolation). The relationship between electric currents and X-ray brightness (and therefore heating) is, however, still debatable. Metcalf et al. (1994) find no correlation between the locations of bright X-ray structures and the sites of sustained strong photospheric currents; the field lines connecting the upward/downward current densities are found to be unassociated with the brightest SXR emission over a 7 day period of observation. For AR 6718, present vector magnetographs like the one in Potsdam are not sensitive enough in the linear polarization to derive electric currents at the feet of the large X-ray loops at which the strength of longitudinal magnetic field is low ($\lesssim$400 G at the magnetograph resolution).

The central part of AR 6718 is formed by a highly sheared magnetic field, with a magnetic shear decreasing progressively with height. This differential shear may be at the origin of the observed loop brightening, triggering a relaxation process as proposed by Heyvaerts & Priest (1984). With the high magnetic Reynolds number of the solar corona, the total magnetic helicity of the magnetic field is preserved. With this constraint, a stressed magnetic field relaxes, via MHD turbulence, to the linear force-free field compatible with the boundary conditions (mainly the photospheric vertical flux distribution). Following Moore et al. (1994), the magnetic shear could be a necessary condition, but not a sufficient one for heating. A differential magnetic shear is likely to be another condition. Finally, a multitude of reconnecting current sheets, the dissipation of a large number of small-scale currents, or a wave heating mechanism are possible alternatives, but the present data cannot permit a definitive selection of all the possible candidates for coronal heating mechanisms.

The authors wish to thank A. Hofmann and H. Aurass for fruitful discussions, B. Kalman for providing the white-light pictures from Debrecen Observatory, J. Harvey for providing the magnetogram from Kitt Peak (the NSO/Kitt Peak data used here are produced cooperatively by NSF/NAO, NASA/GSFC, and NOAA/SEL), and R. Hellier and C. Coutard for the MSDP observations at the Meudon Solar tower. The MSDP observations have been digitalized at the microdensitometer MAMA of the Observatoire de Paris. B. S. thanks the Smithsonian Institute for supporting her stay in Cambridge (US). L. G. was supported in part by NASA grant NAGW-4081 to the Smithsonian Institution.

REFERENCES

Alissandrakis, C. E. 1981, A&A, 100, 197
Antiochos, S. K., Dahlburg, R. B., & Klimchuk, J. A. 1994, ApJ, 420, L41
Aurass, H., Hofmann, A., Magun, A., Soru-Escaut, I., & Zlobec, P. 1993, Sol. Phys., 145, 151
Berger, M. A. 1985, ApJS, 59, 433
Démoulin, P. 1994, in Advances in Solar Physics, ed. G. Belvedere, M. Rodono, & G. M. Simnett (Berlin: Springer), 121
Démoulin, P., Bagalá, L. G., Mandrini, C. H., Hénoux, J. C., & Rovira, M. G. 1996, A&A, submitted
Gary, G. A., & Hagyard, M. J. 1990, Sol. Phys., 126, 21
Gary, G. A., Moore, R. L., Hagyard, M. J., & Haisch, B. M. 1987, ApJ, 314, 782
Golub, L. 1991, in Mechanisms of Chromospheric and Coronal Heating, ed. P. Ulmschneider, E. R. Priest, & R. Rosner (Berlin: Springer), 115
Golub, L., Zirin, H., & Wang, H. 1994, Sol. Phys., 153, 179
Hannakam, L., Gary, G. A., & Teuber, D. L. 1984, Sol. Phys., 94, 219
Heyvaerts, J., & Priest, E. R. 1984, A&A, 137, 63
Livingston, W. C., Harvey, J., Slaughter, C., & Trumbo, D. 1976, Appl. Opt., 15, 40
Martin, S. 1990, in IAU Colloq. 117, Dynamics of Quiescent Prominences, ed. V. Ruzdjak & E. Tandberg-Hanssen (Lecture Notes in Physics, Vol. 363), 1
McClymont, A. N., & Mikic, Z. 1994, ApJ, 422, 899
Mein, P. 1977, Sol. Phys., 54, 44
Metcalf, T. R., Canfield, R. C., Hudson, H. S., Mickey, D. L., Wülser, J. P., Martens, P. C. H., & Tsuneta, S. 1994, ApJ, 428, 860
Metcalf, T. R., Jiao, L., McClymont, A. N., Canfield, R. C., & Uitenbroek, H. 1995, ApJ, 439, 474
Moore, R. T., Porter, J., Roumeliotis, G., Tsuneta, S., Shimizu, T., Sturrock, P. A., & Acton, L. W. 1994, Proc. Kofu Meeting (NRO Rep. No. 360), 89
Peres, G., Reale, F., & Golub, L. 1994, ApJ, 422, 412
Poletto, G., Vaiana, G. S., Zombeck, M. V., Kriefer, A. S., & Timothy, A. F. 1975, Sol. Phys., 44, 83
Rosenbluth, M. N., & Bussac, M. N. 1979, Nucl. Fusion, 19(4), 489
Sakurai, T. 1982, Sol. Phys., 76, 301
Sakurai, T., & Uchida, Y. 1977, Sol. Phys., 52, 397
Sams, B. J. III, Golub, L., & Weiss, N. O. 1992, ApJ, 399, 313
Schmieder, B., Dere, K. P., Raadu, M. A., Démoulin, P., & Alissandrakis, C. E. 1990, Adv. Space Res., 10(9), 195
Schmieder, B., Golub, L., & Antiochos, S. K. 1994, ApJ, 425, 326
Spiller, E., McCorkle, R. A., Wilczynski, J. S., Golub, L., Nystrom, G., Takacs, P. Z., & Welch, C. 1991, Opt. Eng., 30, 1109
Taylor, J. B. 1974, Phys. Rev. Lett., 33, 1139
Van den Oord, G. H. J. 1993, Adv. Space Res., 13(9), 143